Microfluidics and Nanofluidics (2021) 25:78
https://doi.org/10.1007/s10404-021-02477-0

RESEARCH PAPER

Pressure-driven generation of complex microfluidic droplet networks

Tayler M. Schimel[1,2] · Mary-Anne Nguyen[2,3] · Stephen A. Sarles[1] · Scott C. Lenaghan[2,3]

Received: 8 April 2021 / Accepted: 30 July 2021

Abstract
Droplet interface bilayers (DIBs) mimic the cell membrane and provide a model membrane platform for studying basic biophysical processes. This paper demonstrates a pressure-driven microfluidic system for the rapid and automated generation of alternating DIB networks, each comprised of four aqueous nanoliter droplets. The microfluidic device features five inlets, one for the continuous oil phase and four independent aqueous channels for T-junction droplet generation. Droplet production rates are controlled by adjusting the applied pressure of each inlet; therefore, controlling the pattern of droplets produced in the main channel and further stored in a downstream hydrodynamic trapping array. Each trap is designed to capture and hold in place one row of four droplets, forming three interfacial lipid bilayers per network. The potential for greater combinations of droplets in a network enables an increased complexity necessary for performing parallel multiplexed biological assays. We further examined flow behavior in response to changes in resistance of the microfluidic device when using a pressure driven source. This microfluidic system provides a high-throughput method for generating DIB networks of complex droplet patterning.

1 Introduction

Due to the intrinsic complexities of biological membranes and difficulty in designing experiments to interrogate the membrane of single cells, droplet interface bilayers (DIBs) provide an effective tool to study a variety of multifaceted biological processes. DIBs are formed when two aqueous-in-oil lipid-coated droplets are in close enough proximity to allow opposing lipid monolayers to "zip" together and form a lipid bilayer. When three or more droplets are brought together in this way, a DIB network is formed, which provides a higher-order compartmentalized test system for analyzing complex biosystems, such as cell-free bioreactors (Timm et al. 2016; Hori et al. 2017), transmembrane proteins (Friddin et al. 2013; Mattern-Schain et al. 2019), integral membrane ion channels (Allen-Benton et al. 2019; Zhang et al. 2020), and compound screening (Szabo and Wallace 2015; Lee et al. 2018). While the most common method for forming DIBs is manual pipetting, this strategy is severely limited by relatively large droplet sizes and a lack of control over droplet placement, which complicates the formation of DIB networks. While large multi-compartment DIB networks have been formed manually by pipetting and 3D printing (Sarles and Leo 2010; Wauer et al. 2014; Friddin et al. 2016; Booth et al. 2017; Challita et al. 2017), microfluidics offer significant potential to make smaller and more precise droplets, and facile production of DIB networks.

Owing to the ability of microfluidic channels to generate large numbers of consistent picoliter sized droplets (Carreras et al. 2015; Schlicht and Zagnoni 2015; Elani et al. 2016; Nguyen et al. 2016) and the laminar flow environment, microfluidics is an ideal platform for the generation of DIBs and DIB networks. As such, many microfluidic techniques have been developed for creating DIBs within microfluidic devices. Multisomes have been formed by generating alternating aqueous droplets by two opposing T-junctions and then encapsulating asymmetric droplet pairs in an oil droplet using a flow-focusing channel geometry (Elani et al. 2016). Multisomes thus form a DIB between the internal droplet pair, as well as between the inner droplets and the external aqueous phase. Multisomes have been validated as model bioreactors with one encapsulated droplet containing a membrane impermeable compound and the other a membrane

✉ Tayler M. Schimel
tschimel@utk.edu

[1] Department of Mechanical, Aerospace, and Biomedical Engineering, University of Tennessee, Knoxville, TN, USA

[2] Center for Agricultural Synthetic Biology, University of Tennessee, Knoxville, TN, USA

[3] Department of Food Science, University of Tennessee, Knoxville, TN, USA

Published online: 16 August 2021

permeable primary amine with a reaction inducing a fluorescence response. Another strategy used a pressure pump system to generate droplets with a double T-junction joined at a Y-junction to enable alternating droplets (Schlicht and Zagnoni 2015). The alternating droplets were captured by pillars located within the main channel. Further, passive molecular permeation and ion-channel mediated permeation of molecules and ions across the bilayer were confirmed using fluorescent assays. A third approach generated droplets by flow-focusing for creating different sized droplets (300–1500 pL), which were then sorted according to size by deep grooves in the channel and held in place under constant flow by micropillars that outlined the grooves (Carreras et al. 2015). The DIB network size was dictated by the length of the grooves and networks as large as 20 droplets, all of a single droplet type, were assembled. Mass transfer across a 5-droplet network was demonstrated by an enzymatic reaction resulting in a fluorescent response. In another study, two opposing T-junctions were used to create a stream of alternating droplets that were captured in a hydrodynamic trapping array to form DIBs from two droplets of asymmetric composition (Nguyen et al. 2016). Thin film electrodes were deposited at trap locations to obtain in situ current measurements corresponding to bilayer growth. Simultaneous electrical interrogation of 8 DIBs also monitored the insertion of alamethicin peptides into the bilayer. While a few studies have demonstrated the formation of 1:1 alternating droplets of two possible compositions and trapped those droplets for observation of chemical reactions and biological assays, advancing the capabilities of microfluidic DIB networks requires a greater number of droplet compositions and degrees of droplet combinations.

While microfluidics has demonstrated effective formation of DIBs and DIB networks, there is currently a limitation in the complexity of droplet arrays that can be formed from one or two inlets. Relatively simple A/B droplet ordering has been achieved with two inlets (Zheng et al. 2004; Frenz et al. 2008; Niu et al. 2008; Hong et al. 2010; Schlicht and Zagnoni 2015; Surya et al. 2015; Elani et al. 2016; Nguyen et al. 2016; Chen and Carolyn 2017; Taylor et al. 2019); however, to study more complex interactions, such as signal transduction or combinatorial screening, droplet arrays and DIB networks with greater diversity in contents and droplet–droplet pairing are needed. To generate droplets in a microfluidic device, fluids can be driven by a syringe pump or by applied pressure. Syringe pumps have the advantage of a fixed volumetric flow rate; however, they also have a slow response time (seconds to hours) and periodic pulsations. The slow response time make syringe pumps unsuited for advanced droplet patterning because the flow rates and resulting droplet production rates cannot be quickly altered. Alternatively, pressure-driven flow response time is as fast as 40 ms and flow is pulseless, but with the potential of backflow. Two ways in which the complexity of droplet networks can be improved is by increasing the number of droplet-generating channels and by adjusting the droplet pattern. Pressure control systems are able to individually control the flow of numerous fluids simultaneously, allowing for multiple droplet types to be generated independently. Droplet patterns can thus be easily manipulated by driving flow with a pressure-driven pump. The controllability of these systems makes it possible to apply varying sinusoidal pressure waves to multiple independent inlets, resulting in changes in droplet production rates. Different DIB patterns may even be created by applying a sine wave shift between opposing T-junction input pressures. Increasing the number of possible droplet types and allowing for advanced patterning of droplets with a pressure-driven flow system enable the design of microfluidic studies for compound chemical screening, electrical and chemical signaling, and altering chemical or protein concentrations (Bayley et al. 2008; Maglia et al. 2009; Kehe et al. 2019).

We report a pressure-driven microfluidic droplet system for the automated generation of arrays of complex DIB networks, a term that we use to describe linear droplet quartets of controllable droplet ordering. The method utilized T-junction channel geometry and a hydrodynamic trapping array to generate 35 possible droplet combinations of four discrete aqueous types in the dispersed oil phase, a vast improvement on previously described works of two droplet types and simple A/B ordering. A pressure-driven pump system was used to vary the droplet production rate and thus the pattern of droplets produced. The effects of input pressures on the droplet production rates, droplet sizes, and droplet production sequences were examined. Droplets were captured in a downstream hydrodynamic quad-trap array, forming four-droplet networks. Further, a circuit-based model was employed to model the change in flow response as droplets were trapped in the device. This work furthers understanding of pressure-driven droplet production and hydrodynamic trapping for complex DIB networks, which provides a platform for studying complex multicomponent biosystems.

2 Results and discussion

2.1 Microfluidic design

We designed a microfluidic device, comprised of a continuous phase channel, which splits into two channels at the inlet, and two pairs of opposing T-junctions positioned in parallel for generating droplets from four independent inputs (Fig. 1). The channel width was 125 μm, and the channel height was 125 μm across the entire device. Aqueous inlets tapered to 40 μm for better control over droplet size (Saqib et al. 2018). Post-droplet generation, the split continuous

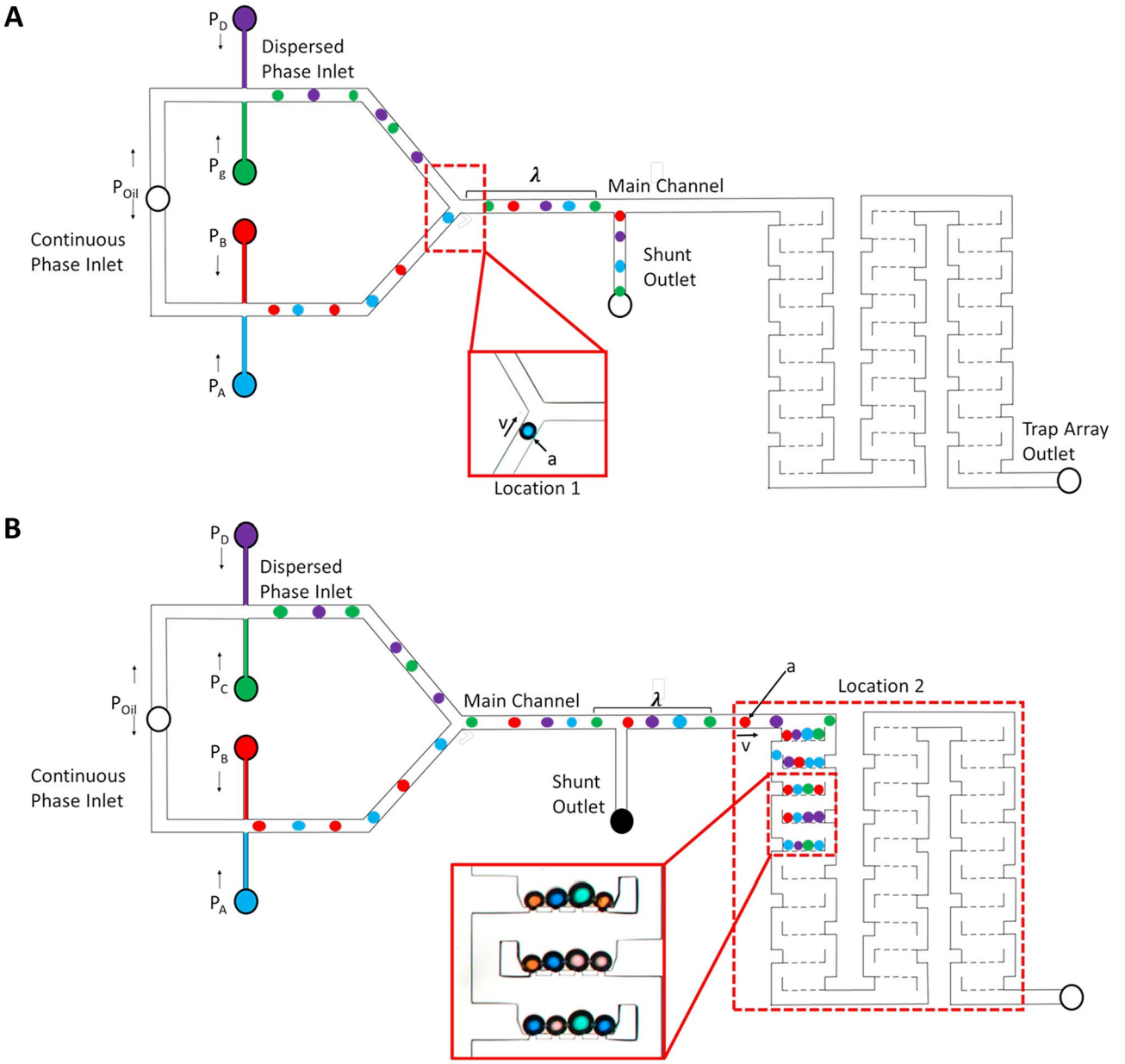

Fig. 1 Schematic of the quad T-junction device generating complex droplet networks under pressure-driven control. **A** While a desired pattern is being established, droplets exit the device through the open shunt channel (left). **B** Once a pattern has been stabilized, the bypass channel is closed and droplets proceed down the main channel to the droplet trapping array. (---) indicates fields of view for shunt open pattern stabilization and shunt closed trapping imaging

phase channels were rejoined by a Y-junction where droplet streams were combined to form the droplet patterns. A bypass channel (shunt), followed the Y-junction and allowed droplets to exit the device when open. Synchronizing droplet production rates is quite challenging; therefore, the shunt was left open prior to trapping to allow internal flow and droplet production to stabilize (Zheng et al. 2004; Schoeman 2014 #433; Hung et al. 2006; Chokkalingam et al. 2008; Frenz et al. 2008; Hong et al. 2010). Input pressures were adjusted manually to synchronize droplet production, prior to the application of a sine wave to alter production rates (Online Resource 2). Once a consistent pattern of droplets at the inlets was established, the bypass channel was closed to route droplets to the trapping array.

The trapping array was a serpentine channel of droplet traps placed in series to form DIB networks for biological studies (Figs. 2, S1), as previously described (Nguyen et al. 2016). Each trap was designed to capture a row of four droplets and was made up of rectangular compartments 440 μm wide, with four 35 μm × 20 μm × 125 μm bleed valves.

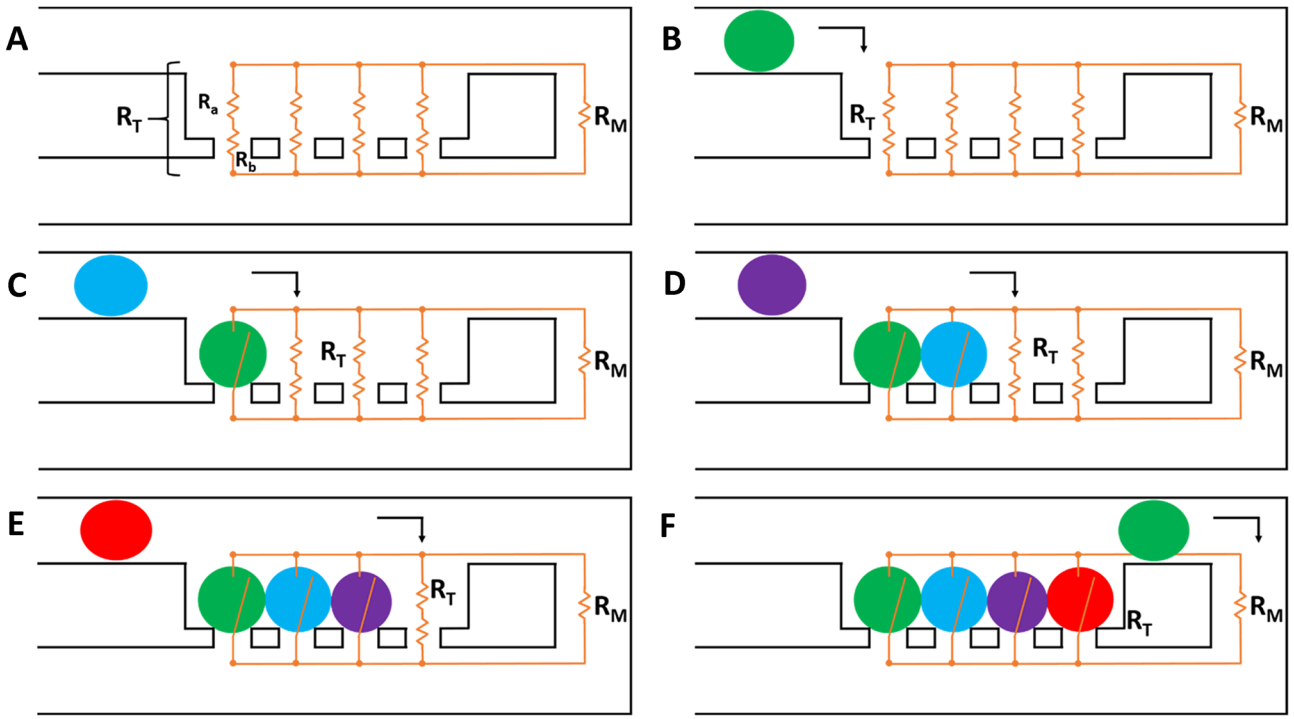

Fig. 2 Schematic of hydrodynamic flow resistances in a 4-droplet trap. **A** Diagram of unfilled trap, where each lane of the unfilled trap has a resistance of $R_T = R_a + R_b$. **B** Droplet 1 enters the trap when R_T is less than the main channel resistance R_M. **C** Droplet 2 enters the open lane of the trap if $R_T < R_M$. **D** Droplet 3 enters the third lane of the trap if $R_T < R_M$. **E** Droplet 4 enters the fourth and last lane of the trap if $R_T < R_M$. **F** Once all four lanes in the trap are filled, R_T becomes greater than R_M and all following droplets in the droplet sequence bypass the filled trap and continue through the main channel

Droplets that enter the trap and block the bleed valves increase the equivalent hydraulic resistance of the trap section. Once a 4-droplet trap filled, the increased resistance caused the following droplets to bypass the filled trap and continue down the main channel to the next unfilled trap. Based on the electrical circuit model (S2), where the resistance of a trap is less than the resistance of the main channel, sequential filling of the trap array was predicted.

2.2 Droplet production rate

All fluid flow was generated by controlling the input pressure using an Elveflow OB1 pressure controller, which enabled individual control of the oil and four separate aqueous solutions. The ratio of aqueous pressure to oil pressure was 1.2–1.9. First, DC input pressures were found by manually adjusting the applied pressure for each aqueous input until an equal number of droplets at the same frequency was generated. A sine wave was then applied to each input with an amplitude of 50–100 Pa above the constant pressure to create fluctuating droplet production rates, higher amplitudes resulted in jetting of the aqueous phases, and lower amplitudes yielded fewer types of droplet combinations. A period of 10 min was chosen because that was approximately the amount of time required to fill 30 traps. Phase shifts of 90°, 120°, 150°, and 180° were applied to each input of opposing T-junction pairs and thus the droplet sequence varied. Droplet sequences were evaluated downstream at the Y-junction, (Fig. 1, Location 1), and the cross-sectional area and velocity of each droplet were calculated (Online Resources 3–6). Cross-flow at the Y-junction pinched off large aqueous droplets (> 1 nL) into multiple droplets; therefore, droplet sizes were measured before the junction. Droplet velocities were measured downstream of the Y-junction, since this was the velocity of the droplets as they entered the trap array. Once a stable pattern was established, the shunt was sealed with tape, routing droplets to the trapping array (Online Resources 7–10).

Droplet production rates, λ, were measured at both Locations 1 and 2 by:

$$\lambda = \frac{1}{\Delta t_d}, \tag{1}$$

where Δt_d was the time between two droplets of the same type. Production rates were measured for every droplet during the time of the experiment. Figure 3 shows the resulting production rate of each droplet type for a 120° phase shift

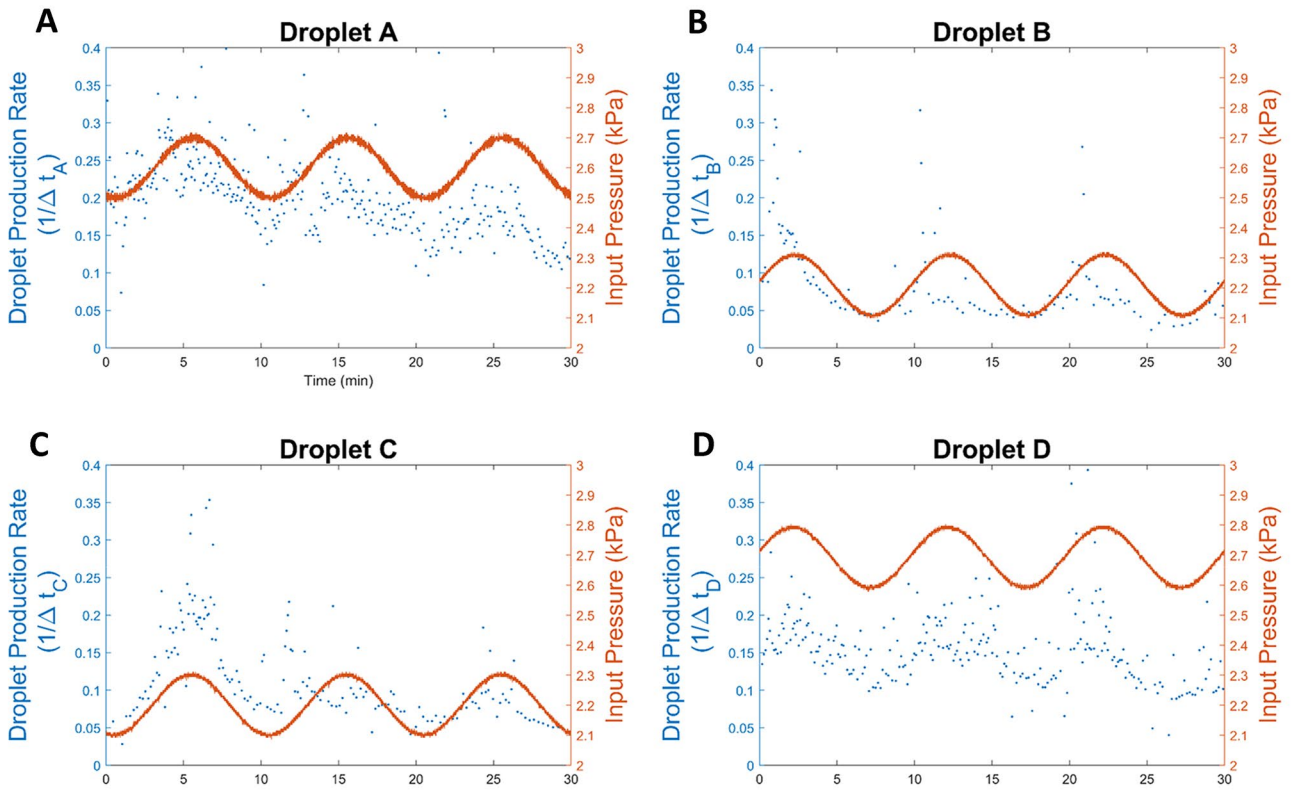

Fig. 3 Droplet sequences are generated by applying sinusoidal pressure waves and thereby altering the droplet production rates. Peak points of droplet productions rates ($\lambda > 0.3\ s^{-1}$) occur by the rapid generation of two droplets of the same type; similarly, low points in droplet production rates ($\lambda < 0.05\ s^{-1}$) occur when there are long pauses between droplet generation. Plots show droplet production rates and input pressures for aqueous input A (**A**), aqueous input B (**B**), aqueous input C (**C**), aqueous input D (**D**). Input pressure waves (orange) and corresponding droplet production rates (blue)

between the A/B and C/D pairs; additional droplet production rates for 90°, 150°, and 180° phase shifts are included in S3.

Droplet production rate is a function of the water-to-oil applied pressure ratio (Lignel et al. 2017). An increase in the pressure applied to the aqueous phase causes an increase in the rate of droplet production, up to the point of jetting. Large pressure differences, up to 200 Pa, in a pair of opposing T-junctions can cause one droplet type to dominate its opposing droplet type and cause the sequences of a single droplet type. Spikes in droplet production rate indicate rapid generation of two droplets of the same type, causing patterns that were less likely to be repeated. Droplet production rates averaged between 0.02 and 0.2 s^{-1} and exhibited a dampening effect of the amplitude over time.

2.3 Droplet size

For both syringe pump and pressure-driven flow, droplet size is predominately controlled by channel geometry. Flow rates and pressure ratio are a second-order determinant of droplet size, although there is a stronger effect with pressure systems (Ward et al. 2005a, b). In the current design, and in agreement with other studies with a constant oil pressure, the acceptable pressure range of the aqueous input for droplet production was very narrow, on the order of 100–200 Pa (Ward et al. 2005a, b; Lignel et al. 2017). When dispersed phase pressure ($\Delta P_{A\text{-}D}$) increased in relation to the continuous phase, droplet size increased, and when $\Delta P_{A\text{-}D}$ was too high, unbroken water flow occurred; if $\Delta P_{A\text{-}D}$ was too low, droplet production ceased. For trapping purposes, droplet size was an important factor. The traps in this study were designed to capture droplets that were 125 µm in diameter. Droplets smaller than the minimum size squeezed through the bleed valve. Larger droplets protruded out of traps, blocking the main channel and increasing the main channel pressure leading to indirect trapping of droplets. To confirm that droplets were in the ideal size range for trapping, droplet cross-sectional area was measured and the equivalent circle diameter was calculated (S4.1). Due to refraction around the perimeter of the droplets, a fraction of the actual droplet size was measured. Therefore, the plotted droplet diameters

were less than the actual and ideal size for trapping. With the microchip's fixed channel geometries, droplet sizes ranged from 18–200 µm to 16–50 µm in equivalent circle diameter when the shunt was open and closed respectively, by varying the relative oil and water applied pressure in Pa (Figs. 4, S4.2–4). Droplet diameters above 65 µm indicate aqueous slugs, which were broken into multiple droplets at the Y-junction, preventing large droplets from entering and disrupting DIB networks in the downstream trap array.

2.4 Droplet patterns

By controlling the aqueous input pressure, and consequently the droplet production rates, the generated droplet sequences were controlled for the purpose of creating complex DIB networks. Droplet sequences were first assessed at viewing Location 1 (Fig. 1) when the shunt was open as a way to preview the patterns that would be captured upon closing the shunt for trapping. Droplet sequences were analyzed by two distinct methods: (1) every droplet in the sequence was considered to be the first of a set of four droplets to create a pattern and (2) the droplet sequence was first split into sets of four droplets and then a pattern was identified for each quartet (Fig. 5). For simplicity, droplet order within a set of four droplets was not considered, thus reducing the number of possible outcomes from 256 permutations down to 35 combinations with repetition. Possible droplet combinations are given in Table 1. The first method, referred to as "all viewed combinations," accounts for any error within the system (i.e. indirect trapping and irregularities in droplet generation) when attempting to predict droplet patterns. For example, if one droplet in the sequence bypassed an open trap and the next four droplets in the sequence were correctly trapped, that pattern would exist in the "all viewed combinations" but not in the ideal patterns. The second method is used for identifying the "ideal" and "trapped" patterns. For all viewed combinations in the shunt open case (SO-AV), droplet sequence was monitored for 30 min, the time required for three sine wave phases, to allow for a baseline standardization of potential patterns (Fig. 6A).

After consistent droplet patterns were established, the shunt was closed and droplets were analyzed at viewing Location 2 (Fig. 1B) for the length of time required to fill the whole trap array (~ 10 min) (Fig. 6B). Fewer droplet quartets were available for analysis in all other cases relative to SO-AV due to the reduced observation time and, therefore,

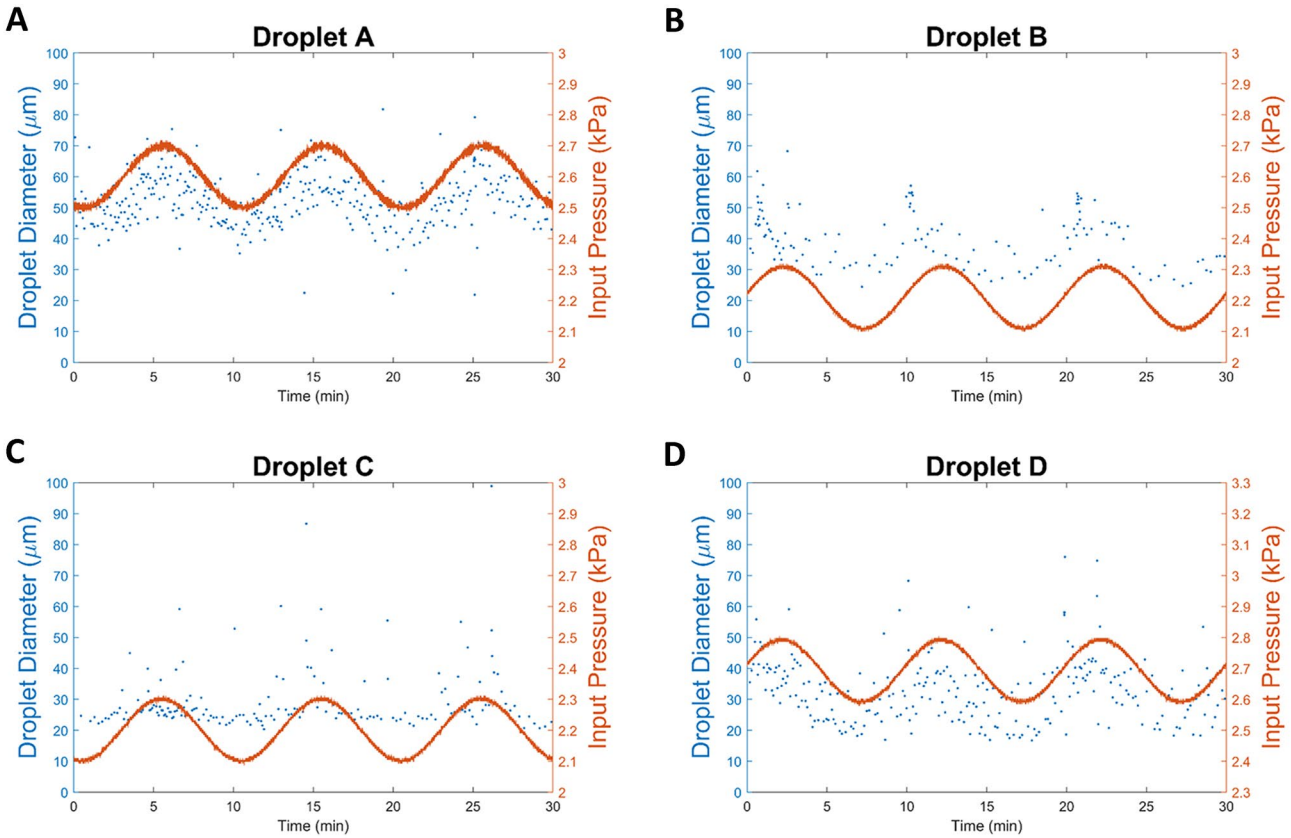

Fig. 4 Droplet size change with applied pressure input. Droplet size is controlled predominantly by channel geometry, but the ratio of aqueous pressure to oil pressure has a minor effect. Plots show droplet diameters and input pressure waves for aqueous input (**A**), aqueous input (**B**), aqueous input (**C**), and aqueous input (**D**). Input pressure waves (orange) and corresponding droplet areas (blue)

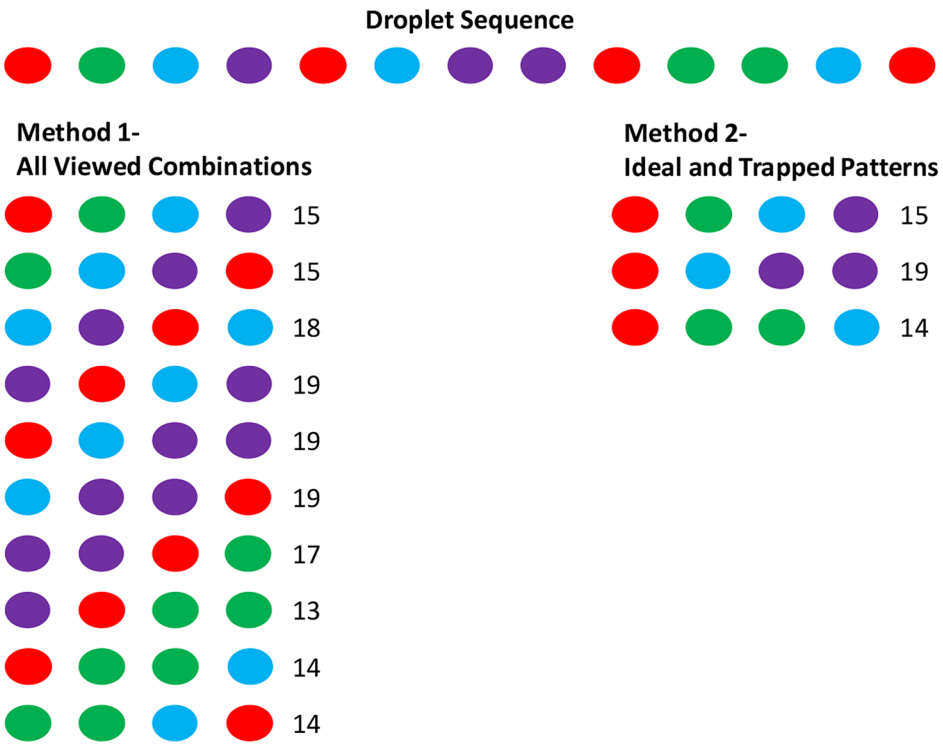

Fig. 5 An example of identifying droplet combinations and patterns from generated droplet sequence. Given a random 13-droplet sequence, droplet patterns were identified by two methods: (1) all view combinations—every droplet in the sequence is taken to be the first in a droplet quartet, resulting in this scenario with 10 droplet combinations, (2) the droplet sequence is first separated into sets of 4 and then patterns are identified from the droplet quartets, in this example the result was 3 droplet patterns. Numbers to the right of each droplet quartet are the combination identification number for each grouping

Table 1 Numbers were assigned to each possible combination of 4 droplets to simplify identification

Combination ID	Droplet Pattern	Combination ID	Droplet Pattern	Combination ID	Droplet Pattern
1		13		25	
2		14		26	
3		15		27	
4		16		28	
5		17		29	
6		18		30	
7		19		31	
8		20		32	
9		21		33	
10		22		34	
11		23		35	
12		24			

accounts for much of the decrease in pattern distribution. If the first droplet in the dataset was the first to be trapped and perfect sequential trapping were to occur, the observed pattern was given by the shunt closed ideal pattern (SC-Ideal) histogram (Fig. 6C). Further, trapped patterns were the droplet patterns that were ultimately observed in the trap array at the completion of the experiment (Fig. 6D). It should be noted that the most prevalent pattern in the 120° shift trapped sample data is again Combination ID #15, which is the pattern most frequent in the original SO-AV data. Combination ID #15 is a DIB network containing one droplet of each of the four droplet types and was the most common pattern to occur in all of the studied phase shifts. This was primarily due to aqueous pressures being balanced prior to each sine wave application, resulting in comparable droplet production rates among the four aqueous inputs.

These experiments were carried out for input pressure phase shifts of 90°, 120°, 150°, and 180° (S5.1–3). Images of the array of trapped droplet networks are shown in S6. Lower phase shifts in input pressure were anticipated to be more consistent, so the 90° shift experiment was conducted three times to demonstrate the repeatability of this method (S7). Values in Table 2 represent the percentage of trapped patterns that match the predictive droplet combination patterns in SC-Ideal, SC-AV, and SO-AV. Only droplet networks containing four droplets at the time point that all traps were filled were counted. As expected, trapped patterns more closely match the SC-Ideal patterns for the lower phase shift scenarios and more errors occurred the greater the phase shift between input pressures. Fluctuations in the size and frequency of droplet production caused indirect trapping and thus errors in pattern prediction (Christopher

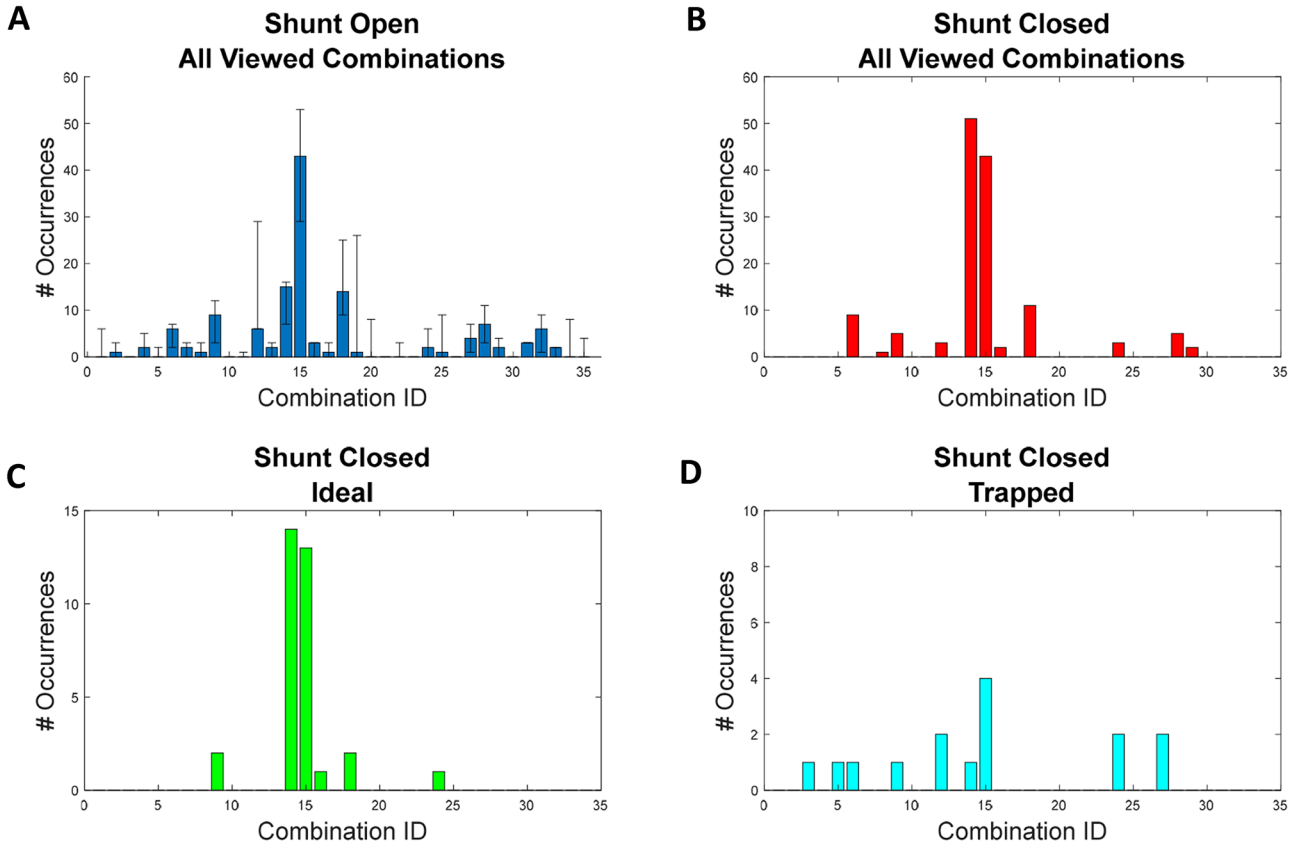

Fig. 6 Generated droplet patterns for 120° pressure shift in the cases of **A** open shunt—all viewed combinations, **B** shunt closed—all viewed combinations, **C** shunt closed ideal pattern, and **D** trapped patterns. All viewed combinations are comprised of four droplets, identified starting with every droplet in the droplet sequence and regardless of order. Ideal patterns are comprised of four droplets, identified by every 4th droplet in the droplet sequence, starting with the first droplet observed after the shunt is closed. These patterns are the droplet combinations that are predicted to be trapped if errorless trapping were to occur in the device. Trapped patterns are droplet combinations that are observed once all traps in the array are filled with four droplets

Table 2 Percentages of observed trapped patterns that match the predictive shunt closed-ideal (SC-Ideal), shunt closed all viewed combinations (SC-AV), and shunt open all viewed combinations (SO-AV)

	Trapped:SC-Ideal (%)	Trapped:SC-AV (%)	Trapped:SO-AV (%)
90° shift	62.46 ± 6.41	81.14 ± 5.71	92.31 ± 0.26
120° shift	53.30	73.33	93.75
150° shift	47.62	52.38	85.71
180° shift	40.0	73.33	80.00

Percentages were calculated by dividing the number of the trapped patterns that correspond to the comparative identified pattern by the total number of trapped patterns

and Anna 2007). Direct trapping and trapping efficiency can be improved by increasing the length of the main channel between traps; however, doing so would increase the resistance of trap array.

2.5 Pressure-driven flow

Shunt channels have been used extensively for droplet sorting with syringe pump systems. The designed shunt was 3 mm in length, giving it a resistance of 4.4×10^4 Pa s μL^{-1}. With the trapping array resistance of 7.6×10^4 Pa s μL^{-1}, droplets preferentially exit the microchip through an open

shunt channel. With the syringe pump droplet production system, the shunt may be closed with little effect on droplet production (Nguyen 2017). In comparison, pressure-driven droplet production results in decreased droplet velocity within the main channel decreasing by 35%, 37%, 57%, and 13% for the 90°, 120°, 150°, and 180° conditions respectively (Fig. 7); droplet velocity also became more uniform after shunt (Table 3). The size of droplets was also shown to significantly decrease and become more uniform upon shunt closure, dropping from an average equivalent circle diameter of 92.7–30.4 µm (Figs. 8, S8.1–3). The greater resistance of the trap array in comparison to the shunt channel caused a decrease in droplet production rate, size, and velocity when using a pressure pump source. This finding was confirmed by the results of the electric circuit model (S9) comparison of flow behavior between syringe pump system and pressure-driven system. Similarly, as the traps were filled, the velocity and size of droplets entering the trap array continued to decrease. The array of captured droplets shown in Fig. S8 of the 120° phase shift data depicts the overall reduction in droplet size, where droplets in the first, second, and third column have an average diameter of 107.6, 97.43, and 72.4 µm, respectively. A consequence of this change in size is that traps at the beginning of the array are most likely to capture fewer than the design-intended 4-droplet network and traps farther along in the array are likely to contain more than four droplets due to incomplete blockage of the bleed valve. This effect can easily be corrected by connecting a flow rate sensor to each fluid input; allowing for flow rate control via pressure. Alternatively, a less expensive solution is to lower the oil pressure as needed while traps are filled: thereby increasing the aqueous to oil pressures ratio and thus the droplet size. Further, the addition of a flow rate sensor would allow for both larger droplet networks and trapping arrays as the increase in pressure experienced as droplets fill the trap array does not negatively impact droplet production in mechanically driven flow.

Table 3 LineFit equations and R^2 values corresponding to droplet velocity graphs in Fig. 7

° Phase shift	Shunt open		Shunt closed	
	LineFit	R^2	LineFit	R^2
90°	$y=1.8E4x+3.9$	0.089	$y=-2.1E3x+2.7$	0.789
120°	$y=3.1E4x+2.4$	0.19	$y=-2.9E3x+1.6$	0.868
150°	$y=5E4x+2.3$	0.538	$y=-1.1E3x+1.1$	0.86
180°	$y=2.2E4x+2.2$	0.168	$y=-3E3x+2.3$	0.894

3 Methods

3.1 Materials

Squalene was purchased from Sigma-Aldrich (UK). 1,2 Diphytanoyl-sn-glycero-3-phosphocholine (DPhPC) and 1,2-dioleoyl-sn-glycero-3-phosphocholine (DOPC) were purchased from Avanti Polar Lipids (Alabama, USA). Aqueous solutions were prepared by mixing food color with DI water. DPhPc and DOPC were dissolved in squalene at concentrations of 2 mg mL^{-1} for initial droplet sequence experiments. DPhPc was dissolved in squalene at a concentration of 6 mg mL^{-1} for trapping experiments.

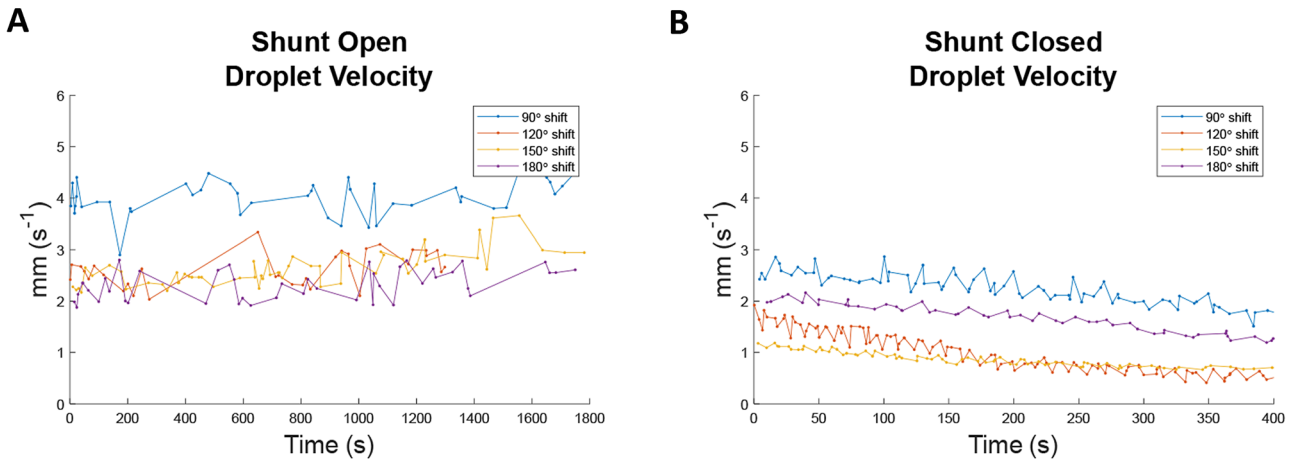

Fig. 7 Plot of individual droplet velocities, **A** droplet velocities when the shunt is open and droplets are freely allowed to exit the device. **B** Droplet velocities when the shunt is closed and droplets are being trapped. Droplet velocity decreased by 13–57% upon shunt closure and slowed further as traps filled

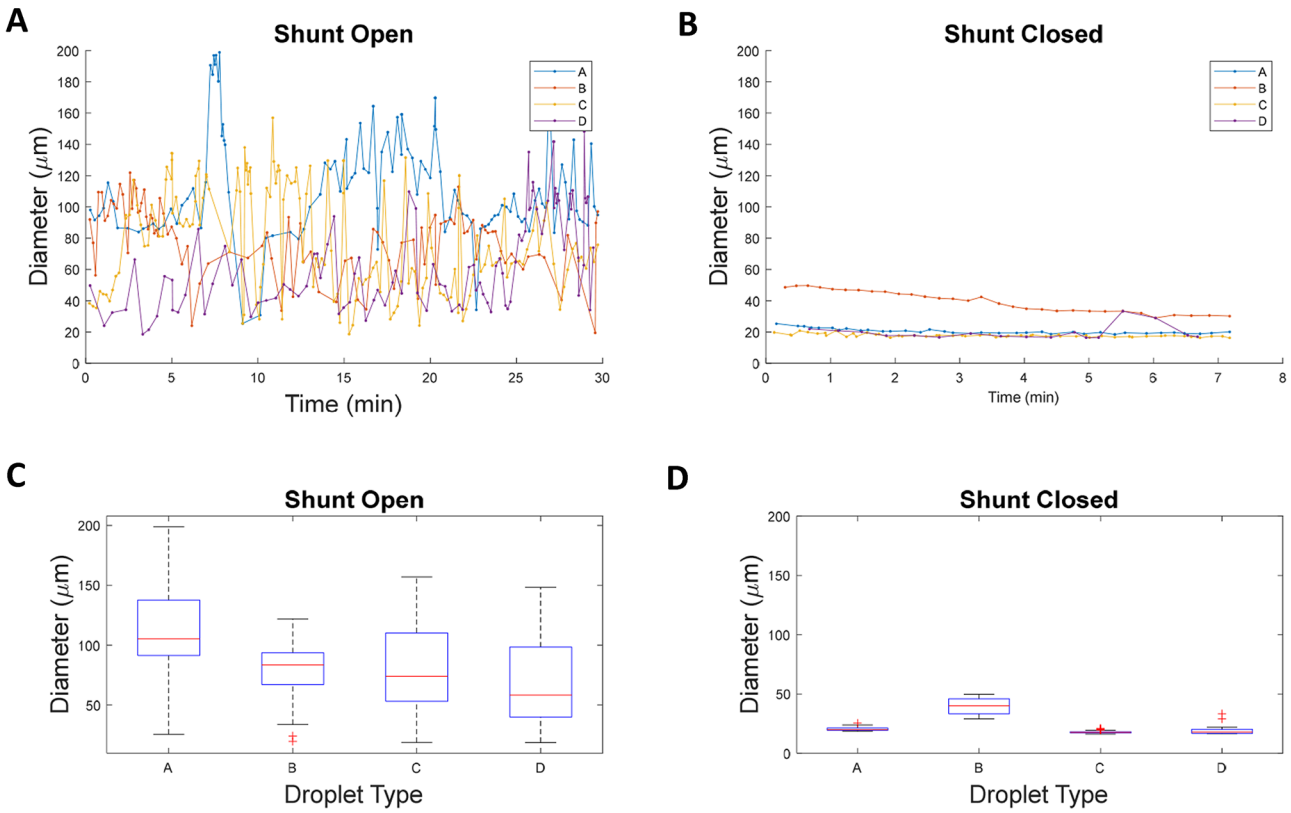

Fig. 8 Measured droplet cross-sectional area for a 120° shift shunt open and shunt closed cases. **A** Droplet size measurements when shunt is open. Droplet size fluctuations are evident. **B** Droplet size measurements when shunt is closed. Droplet size decreases slowly as traps are filled. **C** Droplet size when shunt is open. Droplet size varies greatly and slugs are often produced. **D** Droplet size when shunt is closed. Droplet size is decreased and more consistent, when the shunt is closed

3.2 Device design and fabrication

Two pairs of opposing T-junctions set in parallel were used for droplet production of four aqueous types. The two incoming droplet streams were joined at a Y-junction, routed through microchannels, and captured in an array of hydrodynamic traps. Each trap was designed to capture and hold in place four droplets in a linear chain. Microchannel geometry was optimized for 125 μm diameter droplets.

Microfluidic devices were fabricated using polydimethylsiloxane (PDMS) (Sylgard 184, Dow Corning, USA) and standard soft lithography techniques. Silicone master wafers were produced by spin-coating a silicon wafer with NFR photoresist. The resist was exposed to CD-26 and baked at 120 °C before Bosch etching. To prevent PDMS adhesion to the silicon master, the wafer was silanized by vapor deposition by chlorotrimethylsilane for 24 h. PDMS at a 10:1 ration of base to curing agent, was then poured over the silicon master, degassed in a vacuum desiccator chamber, and cured for at least 2 h at 80 °C. The PDMS devices were cut and then peeled off of the master, and holes were punched at the inlet and outlet ports. PDMS devices were then cleaned and bonded by plasma oxidation to PDMS coated microscope slides. The bonded microchips were heated again at 80 °C for 2 h. It is common for microdroplets to shrink over time due to fluid absorption into PDMS walls. To minimize this effect, microchips were soaked in water for at least an hour before being used for experiments.

3.3 Microfluidic device operation and modeling

Two Elveflow OB1 pressure controllers (Elveflow, France) were used to regulate the applied pressure to the oil and all aqueous phases. All pressures were independently applied in the range of 2–6 kPa. Sampling rates were every 0.05 s for every channel. The system allowed for on-demand generation of droplets at each of the four T-junctions by adjusting the pressure of each phase simultaneously by Elveflow, a computer-controlled software. PTFE tubing and 23 gage blunt stainless steel needles were used to connect the aqueous solution containers to the inlet ports of the microfluidic device.

A confocal microscope (Olympus IX83) was used for all experiments. Images and videos were acquired (up to 58 frames s^{-1}) using an Olympus DP74 color camera and CellSens Demension software. An objective lens of 4 × was used. CellSens Dimension's Count and Measure software and MATLAB were used to analyze and process recorded videos and images. MATLAB Simscape software was used to model the microfluidic device using the electrical circuit analogy. Syringe-pump-driven flow input was modeled as DC current, and pressure-driven flow input was modeled as DC voltage.

4 Conclusions

In this work, we developed and validated a pressure-driven microfluidic system for the generation of complex alternating DIB networks. By varying the pressure waves applied to each of the aqueous inputs, it was possible to "randomize" droplet sequences, with the potential to capture varied combinations of droplets. Combined with the validated quad-trapping arrays, three serially connected DIBs could be formed, providing a platform for communication between droplets. Further, we characterized pressure-driven flow behavior in response to small changes in resistance. In the current design, the velocity at which droplets travel down the main decreased by 13–57% when the shunt was closed; a characteristic that does not match syringe pump-driven flow where flow rate is constant. Droplet velocities continued to decrease as traps in the array were filled and droplet sizes became smaller, indicating that pressure-driven flow was exceptionally sensitive to any increase in resistance. Based on this finding, flow rate sensors may be necessarily coupled with each pressure inputs to counteract this occurrence. This work has furthered the understanding of pressure-driven microfluidic droplet generation and hydrodynamic trapping to facilitate the creation of complex DIB networks for experiments analyzing complex biosystems.

Supplementary Information The online version contains supplementary material available at https://doi.org/10.1007/s10404-021-02477-0.

References

Allen-Benton M, Findlay HE, Booth PJ (2019) Probing membrane protein properties using droplet interface bilayers. Exp Biol Med 244(8):709–720

Bayley H, Cronin B, Heron A, Holden MA, Hwang WL, Syeda R, Thompson J, Wallace M (2008) Droplet interface bilayers. Mol Biosyst 4(12):1191

Booth MJ, Restrepo Schild V, Downs FG, Bayley H (2017) Functional aqueous droplet networks. Mol Biosyst 13(9):1658–1691

Carreras P, Elani Y, Law RV, Brooks NJ, Seddon JM, Ces O (2015) A microfluidic platform for size-dependent generation of droplet interface bilayer networks on rails. Biomicrofluidics 9(6):064121

Challita EJ, Najem JS, Freeman EC, Leo DJ (2017) A 3D printing method for droplet-based biomolecular materials. In: Nanosensors, Biosensors, info-tech sensors and 3d systems 2017, international society for optics and photonics

Chen X, Carolyn (2017) A microfluidic chip integrated with droplet generation, pairing, trapping, merging, mixing and releasing. RSC Adv 7(27):16738–16750

Chokkalingam V, Herminghaus S, Seemann R (2008) Self-synchronizing pairwise production of monodisperse droplets by microfluidic step emulsification. Appl Phys Lett 93(25):254101

Christopher GF, Anna SL (2007) Microfluidic methods for generating continuous droplet streams. J Phys D Appl Phys 40(19):R319

Elani Y, Solvas XCI, Edel JB, Law RV, Ces O (2016) Microfluidic generation of encapsulated droplet interface bilayer networks (multisomes) and their use as cell-like reactors. Chem Commun 52(35):5961–5964

Frenz L, Blouwolff J, Griffiths AD, Baret J-C (2008) Microfluidic production of droplet pairs. Langmuir 24(20):12073–12076

Friddin MS, Morgan H, De Planque MRR (2013) Cell-free protein expression systems in microdroplets: Stabilization of interdroplet bilayers. Biomicrofluidics 7(1):014108

Friddin MS, Bolognesi G, Elani Y, Brooks NJ, Law RV, Seddon JM, Neil MAA, Ces O (2016) Optically assembled droplet interface bilayer (OptiDIB) networks from cell-sized microdroplets. Soft Matter 12(37):7731–7734

Hong J, Choi M, Edel JB, Demello AJ (2010) Passive self-synchronized two-droplet generation. Lab Chip 10(20):2702–2709

Hori Y, Kantak C, Murray RM, Abate AR (2017) Cell-free extract based optimization of biomolecular circuits with droplet microfluidics. Lab Chip 17(18):3037–3042

Hung L-H, Choi KM, Tseng W-Y, Tan Y-C, Shea KJ, Lee AP (2006) Alternating droplet generation and controlled dynamic droplet fusion in microfluidic device for CdS nanoparticle synthesis. Lab Chip 6(2):174

Kehe J, Kulesa A, Ortiz A, Ackerman CM, Thakku SG, Sellers D, Kuehn S, Gore J, Friedman J, Blainey PC (2019) Massively parallel screening of synthetic microbial communities. Proc Natl Acad Sci 116(26):12804–12809

Lee Y, Lee H-R, Kim K, Choi SQ (2018) Static and dynamic permeability assay for hydrophilic small molecules using a planar droplet interface bilayer. Anal Chem 90(3):1660–1667

Lignel S, Salsac A-V, Drelich A, Leclerc E, Pezron I (2017) Water-in-oil droplet formation in a flow-focusing microsystem using pressure- and flow rate-driven pumps. Colloids Surf A Physicochem Eng Asp 531:164–172

Maglia G, Heron AJ, Hwang WL, Holden MA, Mikhailova E, Li Q, Cheley S, Bayley H (2009) Droplet networks with incorporated protein diodes show collective properties. Nat Nanotechnol 4(7):437–440

Mattern-Schain SI, Nguyen M-A, Schimel TM, Manuel J, Maraj J, Leo D, Freeman E, Lenaghan S, Sarles SA (2019) Totipotent cellularly-inspired materials. In: Smart materials, adaptive structures and intelligent systems 59131, American Society of Mechanical Engineers

Nguyen, M-A (2017) High-Throughput Functional System for Encapsulated Networks of Model Cell Membranes. PhD diss., University of Tennessee

Nguyen M-A, Srijanto B, Collier CP, Retterer ST, Sarles SA (2016) Hydrodynamic trapping for rapid assembly and *in situ* electrical characterization of droplet interface bilayer arrays. Lab Chip 16(18):3576–3588

Niu X, Gulati S, Edel JB, Demello AJ (2008) Pillar-induced droplet merging in microfluidic circuits. Lab Chip 8(11):1837

Saqib M, Şahinoğlu OB, Erdem EY (2018) Alternating droplet formation by using tapered channel geometry. Sci Rep 8(1):1606

Sarles SA, Leo DJ (2010) Physical encapsulation of droplet interface bilayers for durable, portable biomolecular networks. Lab Chip 10(6):710

Schlicht B, Zagnoni M (2015) Droplet-interface-bilayer assays in microfluidic passive networks. Sci Rep 5(1):9951

Schoeman R, Kemna E, Wolbers F, van den Berg A (2014) High-throughput deterministic single-cell encapsulation and droplet pairing fusion and shrinkage in a single microfluidic device. ELECTROPHORESIS 35(2-3):385–392. https://doi.org/10.1002/elps.201300179

Surya HPN, Parayil S, Banerjee U, Chander S, Sen AK (2015) Alternating and merged droplets in a double T-junction microchannel. Biochip J 9(1):16–26

Szabo M, Wallace MI (2016) Imaging potassium-flux through individual electropores in droplet interface bilayers. Biochimica et Biophysica Acta (BBA) - Biomembranes 1858(3):613-617

Taylor G, Nguyen M-A, Koner S, Freeman E, Collier CP, Sarles SA (2019) Electrophysiological interrogation of asymmetric droplet interface bilayers reveals surface-bound alamethicin induces lipid flip-flop. Biochim Biophys Acta BBA Biomembr 1861(1):335–343

Timm AC, Shankles PG, Foster CM, Doktycz MJ, Retterer ST (2016) Toward microfluidic reactors for cell-free protein synthesis at the point-of-care. Small 12(6):810–817

Ward T, Faivre M, Abkarian M, Stone HA (2005a) Microfluidic flow focusing: drop size and scaling in pressure versus flow-rate-driven pumping. Electrophoresis 26(19):3716–3724

Ward T, Faivre M, Abkarian M, Stone HA (2005b) Microfluidic flow focusing: drop size and scaling in pressureversus flow-rate-driven pumping. Electrophoresis 26(19):3716–3724

Wauer T, Gerlach H, Mantri S, Hill J, Bayley H, Sapra KT (2014) Construction and manipulation of functional three-dimensional droplet networks. ACS Nano 8(1):771–779

Zhang Y, Bracken H, Woolhead C, Zagnoni M (2020) Functionalisation of human chloride intracellular ion channels in microfluidic droplet-interface-bilayers. Biosens Bioelectron 150:111920

Zheng B, Tice JD, Ismagilov RF (2004) Formation of droplets of alternating composition in microfluidic channels and applications to indexing of concentrations in droplet-based assays. Anal Chem 76(17):4977–4982